

Interacting viscous ghost tachyon, K-essence and dilaton scalar field models of dark energy

K. Karami^{1*}, K. Fahimi²

¹Department of Physics, University of Kurdistan, Pasdaran St., Sanandaj, Iran

²Department of Physics, Sanandaj Branch, Islamic Azad University, Sanandaj, Iran

April 3, 2024

Abstract

We study the correspondence between the interacting viscous ghost dark energy model with the tachyon, K-essence and dilaton scalar field models in the framework of Einstein gravity. We consider a spatially non-flat FRW universe filled with interacting viscous ghost dark energy and dark matter. We reconstruct both the dynamics and potential of these scalar field models according to the evolutionary behavior of the interacting viscous ghost dark energy model, which can describe the accelerated expansion of the universe. Our numerical results show that the interaction and viscosity have opposite effects on the evolutionary properties of the ghost scalar field models.

PACS numbers: 98.80.-k, 95.36.+x

Keywords: Cosmology, Dark energy

*KKarami@uok.ac.ir

1 GDE scenario

The GDE density is proportional to the Hubble parameter [1, 2, 3, 4, 5, 6, 7, 8, 9, 10]

$$\rho_D = \alpha H, \quad (1)$$

where α is a constant. Here we consider a spatially non-flat FRW universe filled with GDE and DM. Within the framework of FRW cosmology, the first Friedmann equation takes the form

$$H^2 + \frac{k}{a^2} = \frac{1}{3M_p^2} (\rho_D + \rho_m), \quad (2)$$

where $M_p = (8\pi G)^{-1/2}$ is the reduced Planck mass. Here $k = 0, 1, -1$ represent a flat, closed and open FRW universe, respectively. Also ρ_D and ρ_m are the energy densities of GDE and DM, respectively.

Using the dimensionless energy densities defined as

$$\Omega_m = \frac{\rho_m}{\rho_{\text{cr}}} = \frac{\rho_m}{3M_p^2 H^2}, \quad \Omega_D = \frac{\rho_D}{\rho_{\text{cr}}} = \frac{\rho_D}{3M_p^2 H^2}, \quad \Omega_k = \frac{k}{a^2 H^2}, \quad (3)$$

the Friedmann equation (2) can be rewritten as

$$1 + \Omega_k = \Omega_D + \Omega_m. \quad (4)$$

Substituting Eq. (1) into $\rho_D = 3M_p^2 H^2 \Omega_D$ yields

$$\Omega_D = \frac{\alpha}{3M_p^2 H}. \quad (5)$$

Using the above relation, the curvature energy density parameter can be obtained as

$$\Omega_k = \left(\frac{9M_p^4 k}{\alpha^2} \right) \left(\frac{\Omega_D}{a} \right)^2 = \left(\frac{\Omega_{k_0}}{\Omega_{D_0}^2} \right) \left(\frac{\Omega_D}{a} \right)^2, \quad (6)$$

where we take $a_0 = 1$ for the present value of the scale factor.

Here, we extend our study to the viscous model of GDE. In the presence of viscosity, the effective pressure of DE takes the form

$$\tilde{p}_D = p_D - 3H\xi, \quad (7)$$

where $\xi = \varepsilon H^{-1} \rho_D$ is the bulk viscosity coefficient in which ε is a constant parameter [11]. A viscosity $\varepsilon > 0$ will be able to drive acceleration [11].

We further assume the viscous GDE interact with DM [12]. In the presence of interaction, the continuity equations are

$$\dot{\rho}_D + 3H(1 + \omega_D)\rho_D = 9\varepsilon H\rho_D - Q, \quad (8)$$

$$\dot{\rho}_m + 3H\rho_m = Q, \quad (9)$$

where $\omega_D = p_D/\rho_D$ is the equation of state (EoS) parameter of the interacting viscous GDE and Q stands for the interaction term. Following [13], we shall assume $Q = 3b^2 H(\rho_m + \rho_D)$ with the coupling constant b^2 .

Taking time derivative of Eq. (1) and using Eqs. (2), (4), (5) and (9) gives

$$\frac{\dot{\rho}_D}{\rho_D} = 3H \left[\frac{\Omega_D - 1 - \frac{\Omega_k}{3} + b^2(1 + \Omega_k)}{2 - \Omega_D} \right]. \quad (10)$$

Taking time derivative of Eq. (5) and using (1) and (10) one can obtain the evolution of the interacting viscous GDE density parameter as

$$\frac{d\Omega_D}{d \ln a} = \left(\frac{3\Omega_D}{\Omega_D - 2} \right) \left[\Omega_D - 1 - \frac{\Omega_k}{3} + b^2(1 + \Omega_k) \right], \quad (11)$$

which is same as that obtained for the interacting GDE in non-flat universe in the absence of viscosity [6]. It is interesting to note that the viscosity constant ϵ does not affect the evolution of the GDE density parameter (11). Substituting Eq. (6) into (11) yields a differential equation for $\Omega_D(a)$ which can be solved numerically with a suitable initial condition like $\Omega_{D_0} = 0.72$. The numerical results obtained for $\Omega_D(a)$ are displayed in Fig. 1 for different coupling constant b^2 . Figure shows that: i) for a given b^2 , Ω_D increases when the scale factor increases. ii) At early and late times, Ω_D increases and decreases with increasing b^2 , respectively.

Substituting Eq. (10) into (8) gives the EoS parameter of the interacting viscous GDE model as

$$\omega_D = \frac{1 - \frac{\Omega_k}{3} + 2b^2 \left(\frac{1 + \Omega_k}{\Omega_D} \right)}{\Omega_D - 2} + 3\epsilon, \quad (12)$$

which shows that in the absence of interaction and viscous terms, i.e. $b^2 = \epsilon = 0$, at early ($\Omega_D \rightarrow 0$) and late ($\Omega_D \rightarrow 1$) times ω_D goes $-1/2$ and -1 , respectively, and cannot cross the phantom divide line [4]. For the present time ($a_0 = 1$), taking $\Omega_{D_0} = 0.72$ and $\Omega_{k_0} = 0.01$ [14] Eq. (12) gives

$$\omega_{D_0} = -0.78 - 2.19b^2 + 3\epsilon, \quad (13)$$

which clears that for $\epsilon = 0$ the phantom EoS parameter ($\omega_{D_0} < -1$) can be obtained provided $b^2 > 0.1$. This value for b^2 is consistent with the recent observations in which we have that b^2 could be as large as 0.2 [15]. Also the phantom divide crossing is in accordance with the observations [16].

The evolution of the EoS parameter (12) for different b^2 and ϵ is plotted in Figs. 2 and 3, respectively. Figure 2 shows that: i) for $b^2 = 0$, ω_D decreases from -0.5 at early times and approaches to -1 at late times. ii) For $b^2 \neq 0$, ω_D increases at early times and decreases at late times. The results of ω_D in the absence of viscosity ($\epsilon = 0$) are in agreement with those obtained by [6]. Figure 3 clears that: i) for a given ϵ , ω_D decreases with increasing the scale factor. ii) For a given scale factor, ω_D increases when ϵ increases.

2 Ghost tachyon model

The tachyon field is another approach for explaining DE. The tachyon energy density and pressure are [17]

$$\rho_T = \frac{V(\phi)}{\sqrt{1 - \dot{\phi}^2}}, \quad (14)$$

$$p_T = -V(\phi)\sqrt{1 - \dot{\phi}^2}. \quad (15)$$

The tachyon EoS parameter yields

$$\omega_T = \frac{p_T}{\rho_T} = \dot{\phi}^2 - 1. \quad (16)$$

To reconstruct the tachyon field via the interacting viscous GDE, equating (12) with (16), i.e. $\omega_D = \omega_T$, gives

$$\frac{1 - \frac{\Omega_k}{3} + 2b^2 \left(\frac{1 + \Omega_k}{\Omega_D} \right)}{\Omega_D - 2} + 3\epsilon = \dot{\phi}^2 - 1. \quad (17)$$

Also equating Eq. (1) with (14), i.e. $\rho_D = \rho_T$, gets

$$\alpha H = \frac{V(\phi)}{\sqrt{1 - \dot{\phi}^2}}. \quad (18)$$

From Eqs. (17) and (18), the kinetic energy and potential of the tachyon field can be obtained as follows

$$\dot{\phi}^2 = \frac{\Omega_D - 1 - \frac{\Omega_k}{3} + 2b^2 \left(\frac{1 + \Omega_k}{\Omega_D} \right)}{\Omega_D - 2} + 3\epsilon, \quad (19)$$

$$V(\phi) = \frac{\alpha^2}{3M_p^2 \Omega_D} \left[\frac{1 - \frac{\Omega_k}{3} + 2b^2 \left(\frac{1 + \Omega_k}{\Omega_D} \right)}{2 - \Omega_D} - 3\epsilon \right]^{1/2}. \quad (20)$$

Note that Eqs. (19) and (20) for the flat case, i.e. $\Omega_k = 0$, and in the absence of viscosity ($\epsilon = 0$) reduce to the results obtained by [8].

From Eq. (19) and using (5), one can get the evolutionary form of the ghost tachyon scalar field as

$$\phi(a) - \phi(1) = \frac{3M_p^2}{\alpha} \int_1^a \Omega_D \left[\frac{\Omega_D - 1 - \frac{\Omega_k}{3} + 2b^2 \left(\frac{1 + \Omega_k}{\Omega_D} \right)}{\Omega_D - 2} + 3\epsilon \right]^{1/2} \frac{da}{a}, \quad (21)$$

where we take $a_0 = 1$ for the present time. The evolution of the ghost tachyon scalar field, Eq. (21), for different values of b^2 and ϵ is plotted in Figs. 4 and 5, respectively. Figures clear that: i) for a given b^2 or ϵ , $\phi(a)$ increases with increasing the scale factor. ii) For a given scale factor, $\phi(a)$ decreases and increases with increasing b^2 and ϵ , respectively. Note that Fig. 4 shows only the real scalar field, i.e. $\dot{\phi}^2 > 0$. Indeed, for $b^2 = 0, 0.02$ and 0.04 the scalar field ϕ becomes pure imaginary ($\dot{\phi}^2 < 0$) at $a > 43.5, 2.8$ and 2.1 , respectively, and it does not show itself in Fig. 4. To investigate this problem in ample detail, the evolution of the ghost tachyon kinetic energy $\chi = \dot{\phi}^2/2$, Eq. (19), for different values of b^2 and ϵ is plotted in Figs. 6 and 7, respectively. Figure 6 confirms that for $b^2 = 0, 0.02$ and 0.04 the kinetic energy becomes negative ($\chi < 0$) at $a > 43.5, 2.8$ and 2.1 , respectively. Figures 6 and 7 show that: i) for a given b^2 or ϵ , the kinetic energy χ decreases when the scale factor increases. ii) For a given scale factor, the kinetic energy decreases and increases with increasing b^2 and ϵ , respectively.

It is worth to note that from Eq. (14) due to having a real tachyon energy density we need to have $\dot{\phi}^2 < 1$ which is in accordance with Figs. 6 and 7. Moreover, from Eq. (16) for $\dot{\phi}^2 < 0$ and $0 < \dot{\phi}^2 < 1$ we have $\omega_T < -1$ and $-1 < \omega_T < 0$, respectively, corresponding to the phantom [18] and quintessence [19] DE, respectively. In the absence of interaction ($b^2 = 0$), the kinetic energy of the ghost tachyon scalar field is always positive (see Fig. 7) and behaves like quintessence DE with $\omega_T = \omega_D > -1$ (see Fig. 3).

The ghost tachyon potential, Eq. (20), versus the scalar field (21) for different b^2 and ϵ is plotted in Figs. 8 and 9, respectively. Figures illustrate that: i) for a given b^2 or ϵ , $V(\phi)$

decreases with increasing ϕ . This behavior is in agreement with the scaling solution $V(\phi) \propto \phi^{-2}$ obtained for the tachyon field corresponding to the power law expansion [20]. ii) For a given scalar field, $V(\phi)$ increases and decreases with increasing b^2 and ϵ , respectively.

3 Ghost K-essence model

The K-essence scalar field model of DE is given by the action [21, 22]

$$S = \int d^4x \sqrt{-g} p(\phi, \chi), \quad (22)$$

where $p(\phi, \chi)$ is the Lagrangian density given by

$$p(\phi, \chi) = f(\phi)(-\chi + \chi^2), \quad (23)$$

and the K-essence energy density is

$$\rho(\phi, \chi) = f(\phi)(-\chi + 3\chi^2). \quad (24)$$

The K-essence EoS parameter takes the form

$$\omega_K = \frac{p(\phi, \chi)}{\rho(\phi, \chi)} = \frac{\chi - 1}{3\chi - 1}. \quad (25)$$

Equating (25) with (12), $\omega_K = \omega_D$, we get

$$\chi = \frac{3 - \frac{\Omega_k}{3} + 2b^2 \left(\frac{1+\Omega_k}{\Omega_D} \right) - \Omega_D + 3\epsilon(\Omega_D - 2)}{5 - \Omega_k + 6b^2 \left(\frac{1+\Omega_k}{\Omega_D} \right) - \Omega_D + 9\epsilon(\Omega_D - 2)}. \quad (26)$$

Using Eq. (26) and $\dot{\phi}^2 = 2\chi$, we obtain the ghost K-essence scalar field as

$$\phi(a) - \phi(1) = \frac{3M_p^2}{\alpha} \int_1^a \Omega_D \left[\frac{6 - \frac{2\Omega_k}{3} + 4b^2 \left(\frac{1+\Omega_k}{\Omega_D} \right) - 2\Omega_D + 6\epsilon(\Omega_D - 2)}{5 - \Omega_k + 6b^2 \left(\frac{1+\Omega_k}{\Omega_D} \right) - \Omega_D + 9\epsilon(\Omega_D - 2)} \right]^{1/2} \frac{da}{a}, \quad (27)$$

which its evolution for different b^2 and ϵ is displayed in Figs. 10 and 11, respectively. Figures present that: i) for a given b^2 or ϵ , $\phi(a)$ increases with increasing the scale factor. ii) For a given scale factor, $\phi(a)$ decreases and increases with increasing b^2 and ϵ , respectively.

The evolution of the ghost K-essence kinetic energy, Eq. (26), for different values of b^2 and ϵ is plotted in Figs. 12 and 13, respectively. Figures clarify that: i) for a given b^2 or ϵ , the ghost K-essence kinetic energy like the tachyon field decreases when the scale factor increases. ii) For a given scale factor, the kinetic energy of the ghost K-essence field like the tachyon model decreases and increases with increasing b^2 and ϵ , respectively. If we compare Fig. 12 with 6 we see that the kinetic energy of the ghost K-essence model in contrast with the ghost tachyon field is always positive. Note that the result of Fig. 12 is in contrast with that obtained by [9] who showed that for a given b^2 , the kinetic energy of the ghost K-essence field increases with increasing the scale factor. This difference may come back to this fact that the K-essence field selected by [9] is a purely kinetic model in which the action (22) is independent of ϕ . This yields the energy density and pressure of a purely kinetic K-essence which are different from those considered in Eqs. (23) and (24).

4 Ghost dilaton model

The pressure and energy density of the dilaton scalar field model are given by [23]

$$p_D = -\chi + ce^{\lambda\phi}\chi^2, \quad (28)$$

$$\rho_D = -\chi + 3ce^{\lambda\phi}\chi^2, \quad (29)$$

where c and λ are constants and $\chi = \dot{\phi}^2/2$. The dilaton EoS parameter takes the form

$$\omega_D = \frac{p_D}{\rho_D} = \frac{ce^{\lambda\phi}\chi - 1}{3ce^{\lambda\phi}\chi - 1}. \quad (30)$$

Equating (30) with (12) gives the solution

$$ce^{\lambda\phi}\chi = \frac{3 - \frac{\Omega_k}{3} + 2b^2\left(\frac{1+\Omega_k}{\Omega_D}\right) - \Omega_D + 3\epsilon(\Omega_D - 2)}{5 - \Omega_k + 6b^2\left(\frac{1+\Omega_k}{\Omega_D}\right) - \Omega_D + 9\epsilon(\Omega_D - 2)}, \quad (31)$$

then with the help of $\chi = \dot{\phi}^2/2$, we obtain

$$e^{\frac{\lambda\phi}{2}}\dot{\phi} = \sqrt{\frac{2}{c}} \left[\frac{3 - \frac{\Omega_k}{3} + 2b^2\left(\frac{1+\Omega_k}{\Omega_D}\right) - \Omega_D + 3\epsilon(\Omega_D - 2)}{5 - \Omega_k + 6b^2\left(\frac{1+\Omega_k}{\Omega_D}\right) - \Omega_D + 9\epsilon(\Omega_D - 2)} \right]^{1/2}. \quad (32)$$

Finally we obtain

$$\phi(a) = \frac{2}{\lambda} \ln \left\{ e^{\frac{\lambda\phi(1)}{2}} + \frac{3M_p^2\lambda}{2\alpha\sqrt{c}} \int_1^a \Omega_D \left[\frac{6 - \frac{2\Omega_k}{3} + 4b^2\left(\frac{1+\Omega_k}{\Omega_D}\right) - 2\Omega_D + 6\epsilon(\Omega_D - 2)}{5 - \Omega_k + 6b^2\left(\frac{1+\Omega_k}{\Omega_D}\right) - \Omega_D + 9\epsilon(\Omega_D - 2)} \right]^{1/2} \frac{da}{a} \right\}. \quad (33)$$

The evolution of the ghost dilaton scalar field (33) for different b^2 and ϵ is displayed in Figs. 14 and 15, respectively. Figures present that: i) for a given b^2 or ϵ , $\phi(a)$ increases with increasing the scale factor. ii) For a given scale factor, $\phi(a)$ decreases and increases with increasing b^2 and ϵ , respectively.

With the help of Eq. (31) we plot the evolution of the ghost dilaton kinetic energy for different b^2 and ϵ in Figs. 16 and 17, respectively. Figures show that for a given b^2 or ϵ , the kinetic energy of the ghost dilaton field like the tachyon and K-essence models decreases with increasing the scale factor.

5 Conclusions

Here we investigated the interacting viscous GDE model in the framework of standard FRW cosmology. For a spatially non-flat FRW universe containing GDE and DM, we obtained the evolution of the fractional energy density and EoS parameters of the interacting viscous GDE model throughout history of the universe. Furthermore, we reconstructed both the dynamics and potential of the tachyon, K-essence and dilaton scalar field models of DE according the evolutionary behavior of the interacting viscous GDE model. Our numerical results show that:

(i) The evolution of the interacting viscous GDE density parameter Ω_D is independent of viscosity constant ϵ . But for a given coupling constant b^2 , Ω_D increases with increasing the scale

factor. Also at early and late times, Ω_D increases and decreases, respectively, with increasing b^2 .

(ii) The EoS parameter ω_D of the GDE model in the absence of viscosity, can cross the phantom divide line ($\omega_D < -1$) at the present provided $b^2 > 0.1$ which is compatible with the observations. Also in the absence of viscosity for a given coupling constant b^2 , ω_D increases and decreases at early and late times, respectively. Moreover, in the absence of interaction for a given viscosity constant ϵ , ω_D decreases when the scale factor increases. For a given scale factor, ω_D increases with increasing ϵ .

(iii) The ghost tachyon scalar field for a given b^2 or ϵ , increases with increasing the scale factor. Also for a given scale factor, it decreases and increases with increasing b^2 and ϵ , respectively. For a given b^2 or ϵ , the ghost tachyon kinetic energy $\chi(a)$ and potential $V(\phi)$ decrease with increasing the scale factor and scalar field, respectively. For a given scale factor, $\chi(a)$ decreases and increases with increasing b^2 and ϵ , respectively. For a given scalar field, $V(\phi)$ increases and decreases with increasing b^2 and ϵ , respectively.

(iv) The ghost K-essence scalar field for a given b^2 or ϵ increases with increasing the scale factor. But its kinetic energy decreases. For a given scale factor, the ghost K-essence scalar field decreases and increases with increasing b^2 and ϵ , respectively. This behavior also holds for the kinetic energy of the ghost K-essence model.

(v) The ghost dilaton scalar field and its corresponding kinetic energy for a given b^2 or ϵ behave like the ghost K-essence model.

All mentioned in above illustrate that the interaction and viscosity have opposite effects on the dynamics of ghost tachyon, K-essence and dilaton scalar field models of DE.

References

- [1] F.R. Urban, A.R. Zhitnitsky, Phys. Rev. D **80**, 063001 (2009);
F.R. Urban, A.R. Zhitnitsky, Phys. Lett. B **688**, 9 (2010);
N. Ohta, Phys. Lett. B **695**, 41 (2011).
- [2] E. Witten, Nucl. Phys. B **156**, 269 (1979);
G. Veneziano, Nucl. Phys. B **159**, 213 (1979);
K. Kawarabayashi, N. Ohta, Nucl. Phys. B **175**, 477 (1980);
C. Rosenzweig, J. Schechter, C.G. Trahern, Phys. Rev. D **21**, 3388 (1980);
P. Nath, R.L. Arnowitt, Phys. Rev. D **23**, 473 (1981).
- [3] M.M. Forbes, A.R. Zhitnitsky, Phys. Rev. D **78**, 083505 (2008).
- [4] R.G. Cai, Z.L. Tuo, H.B. Zhang, arXiv:1011.3212;
R.G. Cai, Z.L. Tuo, Y.B. Wu, Y.Y. Zhao, arXiv:1201.2494.
- [5] E. Ebrahimi, A. Sheykhi, Phys. Lett. B **705**, 19 (2011);
E. Ebrahimi, A. Sheykhi, Int. J. Mod. Phys. D **20**, 2369 (2011);
A. Khodam-Mohammadi, et al., Mod. Phys. Lett. A **27**, 1250100 (2012);
K. Karami, A. Abdolmaleki, arXiv:1202.2278;
K. Saaidi, arXiv:1202.4097;
K. Saaidi, A. Aghamohammadi, B. Sabet, arXiv:1203.4518.
- [6] A. Sheykhi, M. Sadegh Movahed, Gen. Relativ. Gravit. **44**, 449 (2012).
- [7] A. Sheykhi, A. Bagheri, Europhys. Lett. **95**, 39001 (2011).

- [8] A. Sheykhi, M. Sadegh Movahed, E. Ebrahimi, *Astrophys. Space Sci.* **339**, 93 (2012).
- [9] A. Rozas-Fernandez, *Phys. Lett. B* **709**, 313 (2012).
- [10] K. Karami, et al., *Int. J. Mod. Phys. D* **22**, 1350018 (2013);
K. Karami, K. Fahimi, *Class. Quantum Grav.* **30**, 065018 (2013);
F. Adabi, K. Karami, M. Mousivand, *Can. J. Phys.* **91**, 54 (2013).
- [11] W. Zimdahl, D. Pavón, *Phys. Lett. B* **521**, 133 (2001);
W. Zimdahl, D. Pavón, *Gen. Relativ. Gravit.* **35**, 413 (2003);
L.P. Chimento, et al., *Phys. Rev. D* **67**, 083513 (2003).
- [12] O. Bertolami, F. Gil Pedro, M. Le Delliou, *Phys. Lett. B* **654**, 165 (2007).
- [13] D. Pavón, W. Zimdahl, *Phys. Lett. B* **628**, 206 (2005);
H. Kim, H.W. Lee, Y.S. Myung, *Phys. Lett. B* **632**, 605 (2006).
- [14] C.L. Bennett, et al., *Astrophys. J. Suppl.* **148**, 1 (2003);
D.N. Spergel, *Astrophys. J. Suppl.* **148**, 175 (2003);
M. Tegmark, et al., *Phys. Rev. D* **69**, 103501 (2004);
U. Seljak, A. Slosar, P. McDonald, *JCAP* **10**, 014 (2006);
D.N. Spergel, et al., *Astrophys. J. Suppl.* **170**, 377 (2007).
- [15] B. Wang, Y. Gong, E. Abdalla, *Phys. Lett. B* **624**, 141 (2005);
B. Wang, C.Y. Lin, E. Abdalla, *Phys. Lett. B* **637**, 357 (2005).
- [16] D. Larson, et al., *Astrophys. J. Suppl.* **192**, 16 (2011);
E. Komatsu, et al., *Astrophys. J. Suppl.* **192**, 18 (2011).
- [17] A. Sen, *JHEP* **10**, 008 (1999);
A. Sen, *JHEP* **04**, 048 (2002);
A. Sen, *JHEP* **07**, 065 (2002);
E.A. Bergshoeff, et al., *JHEP* **05**, 009 (2000);
T. Padmanabhan, *Phys. Rev. D* **66**, 021301 (2002);
T. Padmanabhan, T.R. Choudhury, *Phys. Rev. D* **66**, 081301 (2002).
- [18] R.R. Caldwell, *Phys. Lett. B* **545**, 23 (2002).
- [19] B. Ratra, J. Peebles, *Phys. Rev. D* **37**, 321 (1988);
R.R. Caldwell, R. Dave, P.J. Steinhardt, *Phys. Rev. Lett.* **80**, 1582 (1998).
- [20] E.J. Copeland, M.R. Garousi, M. Sami, S. Tsujikawa, *Phys. Rev. D* **71**, 043003 (2005).
- [21] T. Chiba, T. Okabe, M. Yamaguchi, *Phys. Rev. D* **62**, 023511 (2000);
C. Armendáriz-Picón, V. Mukhanov, P.J. Steinhardt, *Phys. Rev. Lett.* **85**, 4438 (2000);
C. Armendáriz-Picón, V. Mukhanov, P.J. Steinhardt, *Phys. Rev. D* **63**, 103510 (2001).
- [22] C. Armendáriz-Picón, T. Damour, V. Mukhanov, *Phys. Lett. B* **458**, 209 (1999);
J. Garriga, V. Mukhanov, *Phys. Lett. B* **458**, 219 (1999).
- [23] M. Gasperini, F. Piazza, G. Veneziano, *Phys. Rev. D* **65**, 023508 (2002);
N. Arkani-Hamed, et al., *JCAP* **04**, 001 (2004).

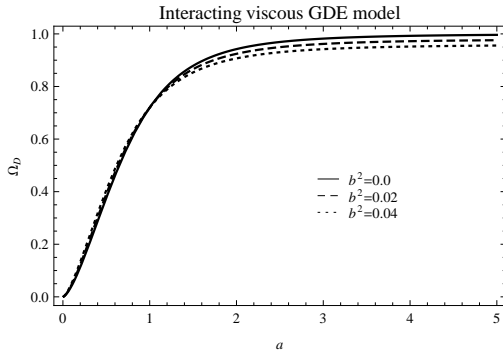


Figure 1: The evolution of the GDE density parameter, Eq. (11), for different coupling constants b^2 . Auxiliary parameters are $\Omega_{D_0} = 0.72$ and $\Omega_{k_0} = 0.01$.

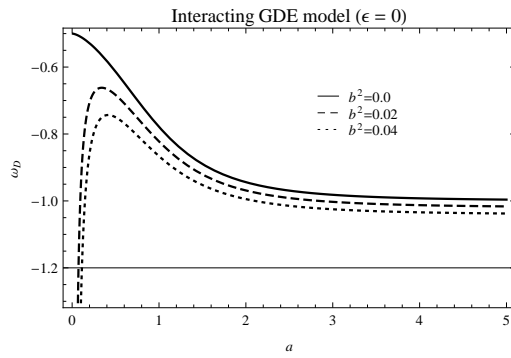


Figure 2: The evolution of the EoS parameter of GDE, Eq. (12), for different coupling constants b^2 with $\epsilon = 0$. Auxiliary parameters as in Fig. 1.

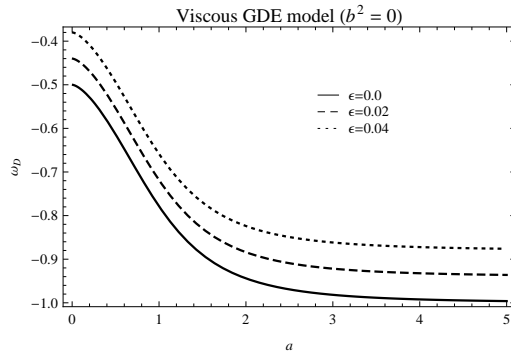


Figure 3: Same as Fig. 2 for different viscosity constants ϵ with $b^2 = 0$. Auxiliary parameters as in Fig. 1.

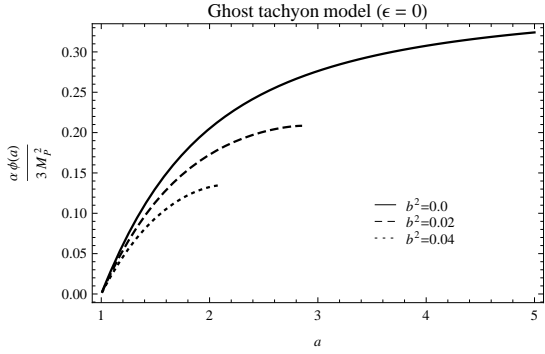


Figure 4: The evolution of the ghost tachyon scalar field, Eq. (21), for different coupling constants b^2 with $\epsilon = 0$. Auxiliary parameters are $\Omega_{D_0} = 0.72$, $\Omega_{k_0} = 0.01$ and $\phi(1) = 0$.

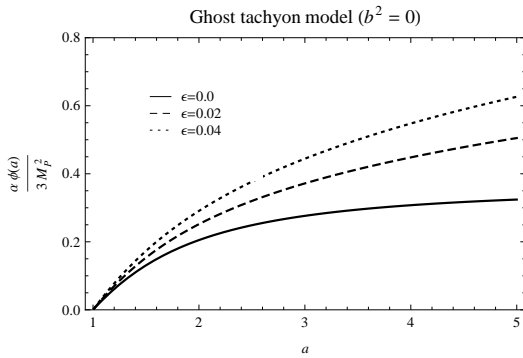


Figure 5: Same as Fig. 4 for different viscosity constants ϵ with $b^2 = 0$. Auxiliary parameters as in Fig. 4.

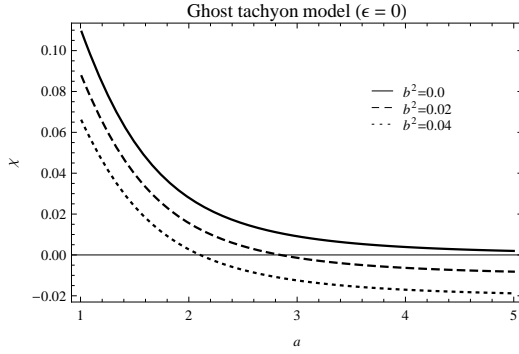


Figure 6: The evolution of the ghost tachyon kinetic energy $\chi = \dot{\phi}^2/2$, Eq. (19), for different coupling constants b^2 with $\epsilon = 0$. Auxiliary parameters as in Fig. 4.

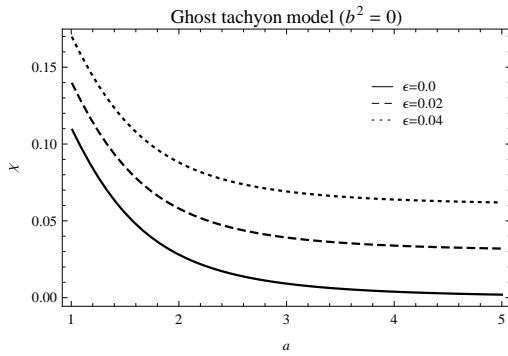


Figure 7: Same as Fig. 6 for different viscosity constants ϵ with $b^2 = 0$. Auxiliary parameters as in Fig. 4.

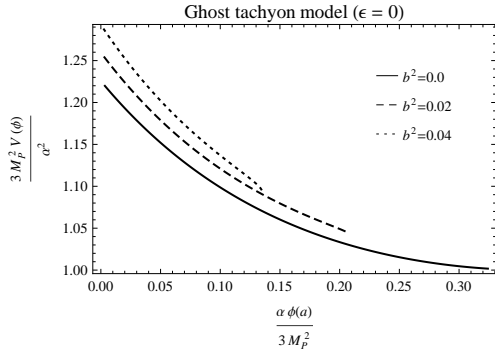


Figure 8: The ghost tachyon potential, Eq. (20), versus the scalar field ϕ for different coupling constants b^2 with $\epsilon = 0$. Auxiliary parameters as in Fig. 4.

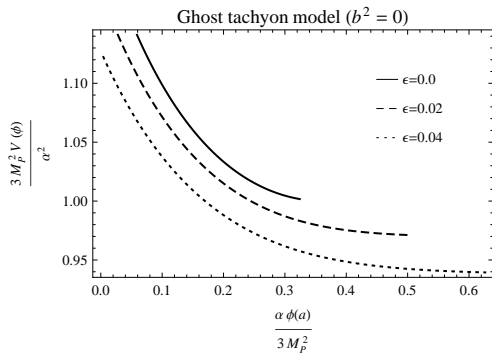


Figure 9: Same as Fig. 8 for different viscosity constants ϵ with $b^2 = 0$. Auxiliary parameters as in Fig. 4.

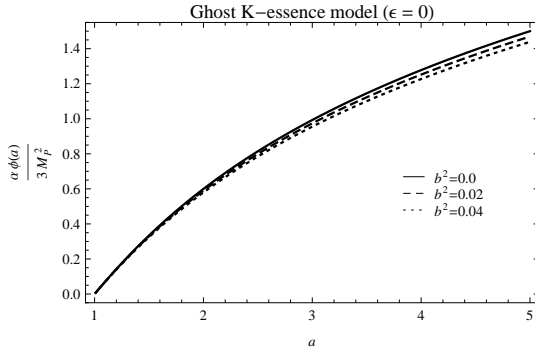


Figure 10: The evolution of the ghost K-essence scalar field, Eq. (27), for different coupling constants b^2 with $\epsilon = 0$. Auxiliary parameters as in Fig. 4.

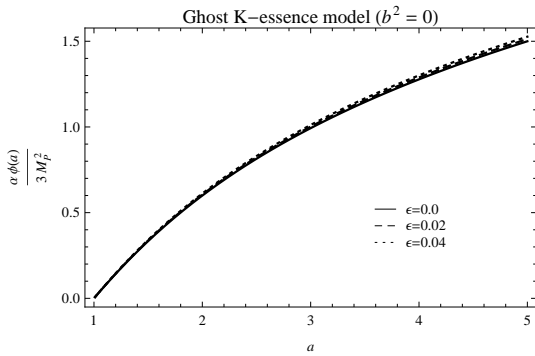


Figure 11: Same as Fig. 10 for different viscosity constants ϵ with $b^2 = 0$. Auxiliary parameters as in Fig. 4.

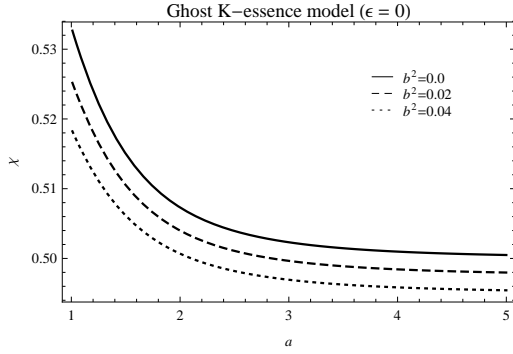


Figure 12: The evolution of the ghost K-essence kinetic energy $\chi = \dot{\phi}^2/2$, Eq. (26), for different coupling constants b^2 with $\epsilon = 0$. Auxiliary parameters as in Fig. 4.

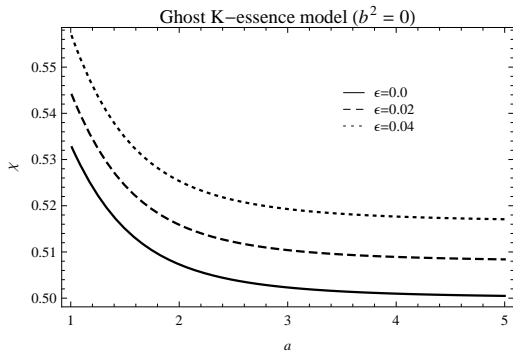


Figure 13: Same as Fig. 12 for different viscosity constants ϵ with $b^2 = 0$. Auxiliary parameters as in Fig. 4.

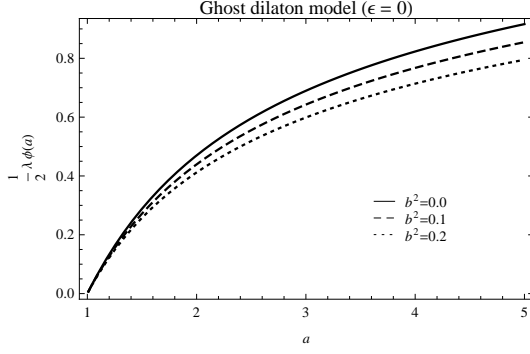


Figure 14: The evolution of the ghost dilaton scalar field, Eq. (33), for different coupling constants b^2 with $\epsilon = 0$. Auxiliary parameters are $\Omega_{D_0} = 0.72$, $\Omega_{k_0} = 0.01$, $\phi(1) = 0$ and $\frac{3M_P^2\lambda}{2\alpha\sqrt{c}} = 1$.

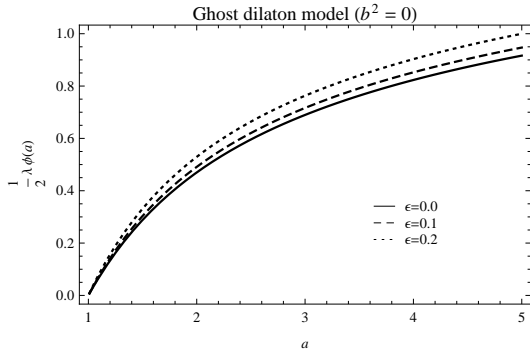


Figure 15: Same as Fig. 14 for different viscosity constants ϵ with $b^2 = 0$. Auxiliary parameters as in Fig. 14.

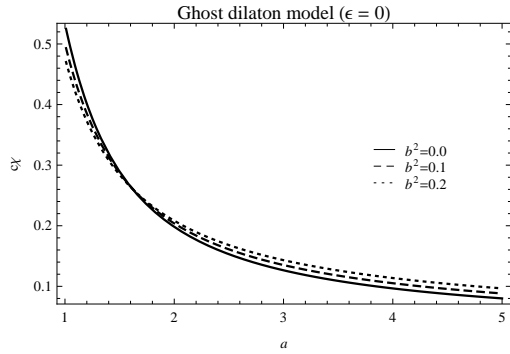


Figure 16: The evolution of the ghost dilaton kinetic energy $\chi = \dot{\phi}^2/2$, Eq. (31), for different coupling constants b^2 with $\epsilon = 0$. Auxiliary parameters as in Fig. 14.

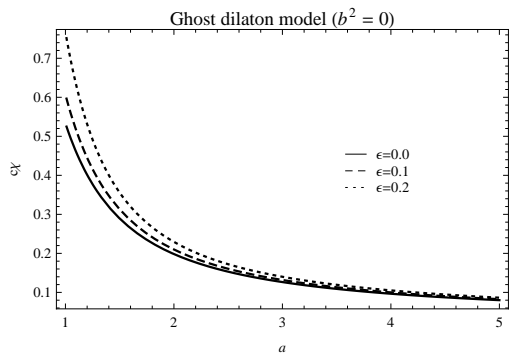


Figure 17: Same as Fig. 16 for different viscosity constants ϵ with $b^2 = 0$. Auxiliary parameters as in Fig. 14.